JOURNAL OF GEOPHYSICAL RESEARCH, VOL. 86, NO. B11, PAGES 10515-10529, NOVEMBER 10, 1981

Phase Relationships of S-Type Granite With H_2O to 35 kbar: Muscovite Granite From Harney Peak, South Dakota

W. L. HUANG

Exxon Production Research, Houston, Texas 77001

P. J. WYLLIE

Department of Geophysical Sciences, University of Chicago, Chicago, Illinois 60637

Muscovite granite (13.8% muscovite, 4.8% normative corundum) was reacted, with varying percentages of H_2O, in cold-seal vessels at 2 kbar and in piston-cylinder apparatus between 10 and 35 kbar. The diagrams illustrating melting/crystallization relationships are: P-T sections with both excess H_2O and with no H_2O added (0.66% H_2O in rock); T-X_{H_2O} sections at 15 kbar and 25 kbar showing H_2O-undersaturated conditions; the H_2O-undersaturated surface for the crystallization of quartz/coesite (small amounts of aluminosilicate minerals persist to higher temperatures). Glass compositions measured by electron microprobe from samples with 5% H_2O at 15 kbar confirm that liquids are syenitic through at least 100°C above the solidus, as predicted from the effect of pressure on the Residua System. Results are explained successfully by phase relationships involving muscovite, quartz, and orthoclase in K_2O-Al_2O_3-SiO_2-H_2O, with reactions depicted in a P_{total}-$P_{e_{H_2O}}$-T model, with special reference to the divariant surfaces in the region $P_{e_{H_2O}} < P_{total}$. With reduced $P_{e_{H_2O}}$ (or a_{H_2O}), produced either by small amounts of H_2O (and H_2O-undersaturation) or by CO_2 + H_2O mixtures, subsolidus dehydration reaction temperatures decrease, vapor-present solidus temperatures increase, and muscovite stability in presence of liquid increases. In general, muscovite, biotite, and amphibole can be precipitated from magmas containing only a few tenths per cent H_2O (although the H_2O-undersaturated liquids coexisting with crystals may contain 3% or more dissolved H_2O). This particular granite cannot be a primary magma from mantle or subducted oceanic crust. It is a possible product of partial fusion of pelitic rocks between about 20 km and 40 km depth given sufficient H_2O, and xenocrystal muscovite or sillimanite from the source rocks. The phase relationships are consistent with the idea of S-type granites, but not sufficient to prove the origin of this rock. Additional tests require phase relationships of other associated granitic rocks, and details of geochemistry, geophysics, and field relationships.

INTRODUCTION

According to *Chappell and White* [1974] and *White and Chappell* [1977], granitic rocks derived by the partial melting of sedimentary rocks contain muscovite and biotite, with no hornblende. These S-type granites contrast with I-type granites, which are derived from igneous source material and characteristically have hornblende more abundant than biotite in mafic samples.

The muscovite granite from Harney Peak, South Dakota, contains abundant muscovite with traces of biotite and no hornblende, and is therefore considered to be of S-type. Phase relationships for this granite have been determined to 35 kbar, with H_2O contents varying from excess to low values. Phase diagrams and some applications have been presented by *Huang and Wyllie* [1973] and *Huang* [1977]. As a basis for interpretation of the phase relationships in the complex rock system, the phase relationships for assemblages of muscovite, sanidine and quartz, with and without aqueous vapor, were determined in the sytem K_2O-Al_2O_3-SiO_2-H_2O [*Huang et al.*, 1973; *Huang and Wyllie*, 1974].

In this paper, we compile the complete phase relationships for the muscovite granite, together with unpublished run data, as representative for an S-type granite. The phase relationships are compared with results from the synthetic system, with special reference to conditions of H_2O-undersaturation. Phase relationships for a biotite granite with mineralogy (and associated granitoid sequences) corresponding to an I-type granite are presented in a companion paper [*Stern and Wyllie*, this issue].

MUSCOVITE GRANITE FROM HARNEY PEAK

The crushed rock sample was kindly supplied by J. J. Norton and R. T. McLaughlin of the U.S. Geological Survey. Table 1 provides a chemical analysis of the rock, its CIPW norm, and a partial mode. Table 2 lists the compositions of alkali and plagioclase feldspar, and muscovite, measured by electron microprobe on grains picked randomly from the crushed rock. The detailed mineralogy and petrology of related pegmatites have been presented by *Norton* [1970].

EXPERIMENTAL PROCEDURES

The powdered rock sample, after passing through 200-mesh sieve, was ground by hand under acetone to grain sizes of 40–60 microns. The sample was dried at 120°C for more than 24 hours before experiments. Samples were sealed within capsules (gold at 2 kbar, silver-palladium or platinum at higher pressures, except for one group of runs in gold at 15 kbar, Table 6) with measured amounts of distilled and deionized water, and reacted in pressure vessels. Runs at 2 kbar were completed in Rene-41 cold-seal pressure vessels with filler rods using standard experimental methods [*Piwinskii and Wyllie*, 1968; *Boettcher and Kerrick*, 1971]. Pressures are accurate to ±5%, and temperatures precise to ±5°C and accurate to ±10°C. Runs at higher pressures were completed in single-stage piston-cylinder apparatus, using the procedures described by *Stern and Wyllie* [this issue], but with some talc

Paper number 1B0494.
0148-0227/81/001B-0494$01.00

TABLE 1. Chemistry, Norm, and Partial Mode of Muscovite Granite (L26) Supplied by J. J. Norton and R. T. McLaughlin

Chemical Composition*	%
SiO_2	74.66
TiO_2	0.03
Al_2O_3	15.55
Fe_2O_3	0.17
FeO	0.42
MnO	0.07
MgO	0.02
CaO	0.42
Na_2O	4.29
K_2O	3.08
H_2O+	0.66
H_2O-	0.04
P_2O_3	0.15
F	0.04
CO_2	0.02
	99.62
O ≡ F	−0.02
Total	99.60
Norm	**%**
Quartz	37.16
Orthoclase	18.20
Albite	36.28
Anorthite	0.98
Hypersthene	0.52
Corundum	4.80
Magnetite	0.25
Ilmenite	0.06
Apatite	0.36
Calcite	0.05
Water	0.70
Partial Mode	**wt %**
Feldspar + quartz	85.2
Muscovite	13.8
Biotite	0.1
Accessory minerals (garnet + apatite + opaque minerals)	0.9

* J. C. DeVine and J. B. Bodkin, analysts.

pieces in the furnace assembly replaced at higher temperatures by pyrex glass to avoid talc dehydration and embrittlement. Pressures are considered accurate to ±5%, and temperatures precise to ±5°C, and accurate to within ±13°C.

In order to avoid metastable melting of the low-pressure mineral assemblage, near-solidus runs at pressures above 15 kbar were performed in two stages, which are indicated in the run tables by pairs of rows. In the first stage the sample was converted to the high-pressure mineralogy, and the temperature was then raised to require run conditions for the second stage. Other two-stage runs from high to low temperatures represent tests for reversibility of the reactions.

Phase assemblages were determined by optical and X ray studies of the quenched materials, using criteria described by *Stern and Wyllie* [this issue]. Muscovite, sillimanite, corundum, and garnet are additional minerals from runs with this rock. Muscovite forms irregular crystal plates about 60 microns in diameter. Sillimanite forms small needles. The high relief of corundum is distinctive. Distinction between alkali feldspar and albitic plagioclase is difficult. The occurrence of two ($\bar{2}01$) peaks on X ray diffraction patterns was taken as evidence for the occurrence of two feldspars. The ($\bar{2}01$) peaks were too weak and broad to be used for estimation of feldspar composition(s). The rare grains of garnet were irregular, about 10–30 microns diameter, similar to those in the original rock. They may represent unreacted original garnets.

Electron microprobe analyses were performed on an ARL EMX electron microprobe at 15 KV, 0.02 micro-amp, and with counting time of 10 s, following the procedures of *Smith* [1965]. The beam size was about 2 micrometers diameter.

MUSCOVITE-ORTHOCLASE-QUARTZ MELTING RELATIONSHIPS

The system K_2O-Al_2O_3-SiO_2-H_2O includes the minerals muscovite, orthoclase, and quartz, and it therefore provides a good model for the natural granite, which is composed of muscovite, two feldspars, and quartz. *A. B. Thompson* [1974] has evaluated theoretically the effect of adding albite as a component to the mica-orthoclase reactions in this system.

Figure 1 shows univariant reactions for the dissociation and melting of muscovite in association with quartz, alkali feldspar, and aluminous minerals in the system K_2O-Al_2O_3-SiO_2-H_2O. The dehydration curve for muscovite extends through Q_3 and Q_4 to Q_2, and that for muscovite + quartz terminates at Q_1. Melting begins at Q_2 and Q_1, respectively.

There are three melting reactions involving muscovite that rise to higher pressures from Q_2, and three melting reactions involving muscovite and quartz that rise from Q_1. The lowest-temperature reactions associated with each of these invariant points has the familiar shape for silicate-H_2O melting curves, with significant depression of melting temperatures caused by increase in pressure. Above each invariant point muscovite is stable, but below each invariant point the corresponding melting curve has muscovite replaced by anhydrous products of the dehydration reactions. The highest-temperature melting reaction associated with each invariant point is the vapor-absent fusion of muscovite, or of muscovite + quartz, which extends above the invariant point with little change in slope compared with the corresponding dehydration reaction at lower pressures and temperatures. The equivalent melting reactions with excess H_2O occur at somewhat lower temperatures, but with the same positive slope (dP/dT).

The estimated compositions of liquids for the vapor-present reactions were illustrated by *Lambert et al.* [1969] and *Wyllie*

TABLE 2. Average Electron Microprobe Analyses for Feldspars and Muscovite in Muscovite Granite (L26)

Minerals	Alkali-Feldspar (4 Grains)	Plagioclase (4 Grains)	Muscovite (2 Grains)
SiO_2	64.6	67.7	45.6
TiO_2	<0.05	<0.05	0.06
Al_2O_3	18.6	20.3	36.0
FeO	0.4	0.3	1.7
MgO	0.05	<0.05	0.7
CaO	0.05	0.8	<0.05
Na_2O	0.8	10.8	0.5
K_2O	16.2	0.05	10.8
Total	100.7	100.0	95.3*
Mole %			Mole %
An	0.3	5.1	Ms 93.3
Ab	6.4	94.3	Pa 6.7
Or	93.2	0.6	

Abbreviations: An—anorthite, Ab—albite, Or—orthoclase, Ms—muscovite, Pa—paragonite.

* H_2O contents in muscovite are not included in total.

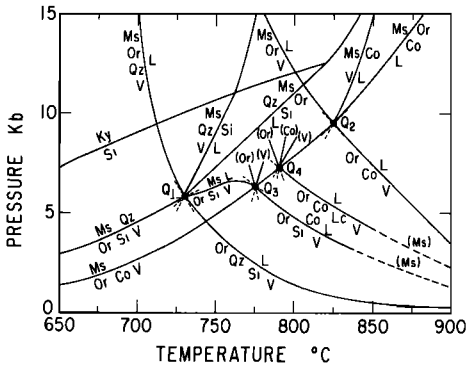

Fig. 1. Univariant reactions in the K_2O-Al_2O_3-SiO_2-H_2O according to *Huang and Wyllie* [1974, Figure 3], incorporating the experimental results of *Huang et al.* [1973]. The reactions of interest in this paper are the dehydration and melting reactions around invariant points Q_1 and Q_2. Abbreviations for Figure 1 and other figures and tables: Ms = muscovite, Qz = quartz, Or = orthoclase, or alkali feldspar, or any polymorph of $KAlSi_3O_8$, Si = sillimanite, Ky = kyanite, Co = corundum, L = liquid, V = vapor, Pl, Ab = plagioclase, Fsp = feldspar, Jd = jadeite, Ga = garnet, Ct = coesite, OrH = orthoclase hydrate.

[1977*a*, Figure 2]. The H_2O-saturated liquid coexisting with orthoclase + quartz + muscovite occurs at a slightly lower temperature than the H_2O-saturated liquid coexisting with orthoclase + quartz [*Huang and Wyllie*, 1974], and it contains a small excess of Al_2O_3 compared with the latter liquid.

For bulk compositions with sufficient H_2O to form muscovite, but with none left over for a vapor phase, melting begins at temperatures higher than the vapor-present reactions. The muscovite reacts to release H_2O which generates H_2O-undersaturated liquid.

Experimental Results

Phase Relationships With Excess H_2O

The runs listed in Table 3 bracket boundaries for the phase diagram in Figure 2. The main features correspond closely to those described and reviewed for biotite granite by *Stern and Wyllie* [this issue, Figure 1], with addition of the muscovite-out curve instead of the biotite-out curve, and of fields for kyanite and metastable corundum.

The subsolidus assemblage at crustal pressures corresponds to that of the natural rock, two feldspars, quartz, and muscovite, with a trace of garnet. At high pressures, this becomes jadeite + coesite + muscovite via reactions plotted in Figure 2. Orthoclase disappears by reaction with aqueous solution between 15 kbar and 25 kbar. Similarly, in the biotite granite, biotite dissolves in the subsolidus vapor between 5 kbar and 10 kbar. in contrast, the muscovite in our rock exists to the highest pressures attained. The traces of accessory garnet were not observed in runs at pressures of 20 kbar or higher, nor in runs more than 25°C above the solidus, but we have not determined a phase boundary that we could draw with confidence.

The solidus curve is identical within the limits of experimental error with those for biotite granite and the synthetic granite system [*Huang and Wyllie*, 1975] to 30 kbar, but it is somewhat higher at 35 kbar. The solidus temperature at high pressures varies as a function of H_2O content (see Figure 5), which might be responsible for the temperature difference.

At 10 kbar and 30 kbar the muscovite-out curve is at 25°C and 40°C, respectively, below the univariant melting curve for muscovite + quartz with excess H_2O, which is explained by the paragonite component of the natural mica (Table 2). At 2 kbar, however, the muscovite persisted in 4-month runs to temperatures about 50°C higher than the maximum stability limit of muscovite + quartz (Figure 1; *Huang and Wyllie* [1974, Figure 2]. This is testimony to slow reaction rates in granitic systems at crustal pressures.

Quartz or coesite is the liquidus phase for the biotite granite, and the corresponding boundary for muscovite granite is shown by the heavy line in Figure 2. Kyanite and sillimanite are produced near the muscovite-out boundary, and traces of kyanite, sillimanite, and corundum occupy large fields above the heavy line. Traces of corundum at 10 kbar and 15 kbar, instead of or accompanying the Al_2SiO_5 polymorph, are considered to be metastable. Corundum, once formed metastably, persists indefinitely in the synthetic muscovite system [*Huang and Wyllie*, 1974].

The change in slope of the solidus curve is associated with the formation of jadeite from plagioclase. The change in slope of the liquidus curve and the increasing width of the melting interval with increasing pressure are functions of the change in composition of the eutectic liquid away from SiO_2. These observations were reviewed in detail by *Stern and Wyllie* [this issue].

Details of the problems and procedures for establishing reversibility of phase boundaries for rock samples within narrow temperature limits were reviewed by *Stern and Wyllie* [1975]. We have discussed the persistence of metastable muscovite at 2 kbar, and the formation and persistence of metastable corundum at 10 kbar and 15 kbar. At higher pressures reaction rates are improved. At 15 kbar, the quartz and muscovite boundaries were reversed within 25°C (Table 3, runs 231, 229, and 242R). At 25 kbar, the kyanite boundary was reversed within 25°C (Table 3, runs 212, 209, 215R, and 217R).

Phase Relationships With No Added H_2O

The runs listed in Table 4 bracket boundaries for the phase diagram in Figure 3. The subsolidus assemblage below the jadeite reaction boundary is the same as in Figure 2, but without vapor. With increasing pressure, plagioclase and quartz are replaced by jadeite and coesite, respectively. Alkali felspar remains stable to high pressures in the absence of vapor. The original garnet was detected in all subsolidus runs.

Melting begins where muscovite reacts releasing H_2O for solution in a small amount of H_2O-undersaturated liquid. The muscovite dissolves completely within 20°C above the solidus, and the melting curve for synthetic muscovite + quartz without vapor is about 25°C higher (Figure 1). This temperature difference is explained by paragonite in the natural muscovite (Table 2). The solidus curve (and the narrow interval for the melting of muscovite) occurs at a temperature higher than the vapor-present muscovite-out curve in Figure 2, and the divergence increases with increasing pressure. This difference corresponds to the difference between fusion curves for muscovite + quartz with and without vapor in Figure 1.

According to Figure 2, the muscovite + quartz dehydration reaction crosses the granite-H_2O solidus near 2 kbar and 660°C. By analogy with the reactions near Q_2 in Figure 1, both solidus and muscovite-out curve for vapor-absent granite should also occur near 660°C and 2 kbar. In fact, the muscovite does not react to produce liquid until 725°C (Table 4), even after runs of 7 months duration. We attribute this to slow reaction at these low pressures in the nearly dry system (see

TABLE 3. Experimental Runs for Muscovite Granite (L26) With Sufficient Water for Vapor to be Present

Run	Pressure, kbar	Temperature, °C	Wt. %, H_2O	Duration, Hours or Months (m)	Results *V* in Every Run
10	2	650	7.2	4 (m)	Qz, Ab, Or, Ms, Ga
12	2	675	9.4	4 (m)	Qz, Ab, Or, Co, (L), Ms?
17	2	700	8.6	3 (m)	Qz, Ab, L, (Si)?
13	2	725	8.1	2 (m)	Qz, L, (Si)?
15	2	750	8.8	2 (m)	Qz, L, (Si)?
14	2	775	8.4	2 (m)	L, (Si)?
16	2	800	8.9	1.5 (m)	L, (Si)?
11	2	850	8.5	1 (m)	L, Co?
225	10	605	31	9	Qz, Ab, Or, Ms, Ga
214	10	615	31	9	Qz, Ab, Or, Ms, Ga
202	10	625	22	11	Qz, Ab, Ms, Ga, L
228	10	700	38	26	Qz, Ms, L
224	10	725	27	25	Co, L, (Si)?
222	10	750	32	21	(Co), L, (Si)?
203	10	800	28	21	(Co), L
201	10	850	27	9	(Co), L
220	10	900	33	12	(Co), L
226	15	600	27	9	Qz, Ab, Or, Ms, Ga
227	15	610	29	9	Qz, Ab, (Or), Ms, Ga, (L)
270	15	635	38	16	Qz, Ab, Ms, (Ga), L
271	15	660	35	16	Qz, Ms, L
240R	15	825	36.3	6	...
	15	700	...	16	Qz, Ms, L
231	15	725	32	26	Qz, Ms, L
242R	15	825	37.3	6	...
	15	725	...	18	Qz, (Ms), L
229	15	750	40	24	Co, (Ky), L
395	15	750	43	12	Co, (Ky), L
219	15	775	46	21	Co, (Ky), L
223	15	800	32	21	(Co), L
210	15	825	45	13	(Co), L
328	20	750	40	24	Qz, Ms, L
321	20	775	40	24	Qz, Ky, L
235	20	800	40	24	Ky, L
208	20	875	46	11	L
213	20	900	52	39	L
237	25	595	24.5	6	Qz, Jd, (Or), Ms
327	25	655	25	13	Qz, Jd, (Or), Ms
248T	25	595	25	6	...
	25	675	...	11.5	Qz, Jd, Ms, (L)
250T	25	595	25	6	...
	25	690	...	10	Qz, Jd, Ms, L
349	25	715	25	19	Qz, Ms, L
317T	25	595	25	6	...
	25	720	...	16	Qz, Ms, L
244T	25	595	25	6	...
	25	745	...	10	Qz, Ms, L
366	25	770	50	24	Qz, Ms, Ky, L
243T	25	595	46	6	...
	25	790	...	18	Qz, Ky, L
381	25	810	32	8	Ky, L
376	25	835	32	13	Ky, L
380	25	840	50	13	Ky, L
304	25	855	33	18	Ky, L
207	25	875	42	13	Ky, L
373	25	900	28	15	Ky, L
212	25	900	50	19	Ky, L
314	25	900	32	15	L
215R	25	975	45	6	...
	25	900	...	16	Ky, L
209	25	925	47	11	L
217R	25	975	55	5	...
	25	925	...	15	L
211	25	950	51	10	L
221	25	975	48	5	L
333T	35	575	20	4	...
	35	700	...	20	Ct, Jd, (OrH), Ms
334T	35	575	20	4	...
	35	725	...	4	Ct, Jd, (OrH), Ms
335T	35	575	20	4	...
	35	750	...	7.5	Ct, Jd, Ms, (L)
350T	35	575	25	18	...
	35	775	...	24	Ct, Jd, Ms, Ky, L
332	35	800	45	18	Ct, Ky, L

TABLE 3. (continued)

Run	Pressure, kbar	Temperature, °C	Wt. %, H_2O	Duration, Hours or Months (m)	Results *V* in Every Run
364T	35	575	49	4	...
	35	825	...	18	Ct, Ky, L
331	35	875	45	10	Ct, Ky, L
399	35	890	35	6	Ct, Ky, L
336	35	900	40	25	Ct, Ky, L
330	35	925	45	10.5	(Ky), L

Abbreviations: see Figure 1. ( ) indicates trace amounts of phase. Runs occupying double rows were completed in two states: T—after holding the sample at subsolidus (or near-solidus) conditions indicated in the first row, it was transferred to conditions at higher temperature indicated in the second row. R—after holding the sample above the liquidus at conditions indicated in the first row, it was transferred to conditions indicated in the second row.

the variety of published curves for muscovite + quartz dehydration in *Huang and Wyllie* [1974, Figure 2]). The solidus at 2 kbar is therefore drawn through the bracket determined by the vapor-present runs of Figure 2, which established that muscovite + quartz should release H_2O for melting at this temperature.

The dashed line is a solidus between 3 kbar and 10 kbar presented by *Brown and Fyfe* [1970] for a granite with 10% and 50% muscovite added to it. The muscovite was slightly more sodic than that in our rock. The agreement in position of the solidus is good.

At 35 kbar, no liquid could be detected in runs up to about 100°C higher than the muscovite-out curve, indicating that the H_2O released from muscovite did not become available for melting. The reaction curve for the formation of $KAlSi_3O_8 \cdot H_2O$ [*Seki and Kennedy*, 1964] fits the experimentally determined solidus at 35 kbar. Therefore, although we could not detect sanidine hydrate in the subsolidus runs, we conclude that H_2O from the muscovite did react with the orthoclase to produce this mineral. The solidus curve therefore follows the sanidine hydrate reaction curve about 32 kbar, and melting begins where this mineral releases H_2O, as shown by the heavy line.

Only a trace of liquid is formed near the solidus. The plagioclase-out curve gives the limit for the coexistence of two feldspars, which are replaced by a single alkali feldspar at higher temperatures. There is no significant increase in amount of liquid through an interval of about 250°C, until the alkali feldspar dissolves, near the Fsp-out curve. Note the distribution of kyanite and metastable corundum produced from the muscovite melting reaction (quartz and corundum are incompatible, see Figure 1). The heavy line representing the liquidus is defined at temperatures where there is a significant decrease in the percentage of quartz. Very small, scattered

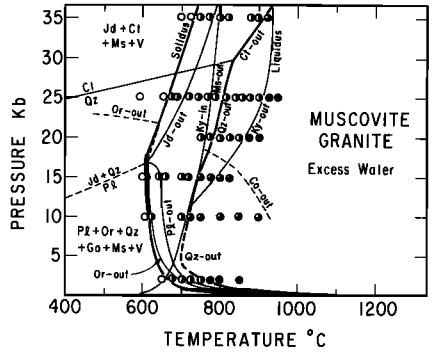

Fig. 2. Phase relations for muscovite granite (L26) with excess water [*Huang and Wyllie*, 1973]. Experiments are listed in Table 3. At pressures below about 1 kbar, a single feldspar should replace Pl + Or at temperatures above the solidus. Abbreviations: see Figure 1.

grains of quartz persist above this boundary, as well as traces of corundum. We interpret this as incomplete reaction in a sluggish system with liquid containing a maximum of 0.6% H_2O. Attempts to reverse the liquidus boundary were unsuccessful (Table 4, runs 263 and 296R), which is disappointing but not unexpected.

Phase Relationships With Variable H_2O Content

The runs listed in Table 5, together with runs from Tables 3 and 4, bracket boundaries for isobaric T-X_{H_2O} sections for the rock-H_2O system at 15 kbar and 25 kbar, as illustrated in Figures 4 and 5. These diagrams show the relationships between the two limits of excess and no additional H_2O illustrated in Figures 2 and 3, and the results are extrapolated further towards the anhydrous rock composition. The composition of the rock is shown by the arrow, at 0.6% H_2O.

The subsolidus phase assemblage at 15 kbar corresponds to the original rock mineralogy, but plagioclase would be replaced by jadeite below about 525°C. At 25 kbar, the jadeite field has expanded to exceed the solidus, and none of the original garnet or orthoclase was observed in runs contining 5% or more H_2O (Figure 5). The capability of only 5% H_2O to dissolve all of the orthoclase (probably incongruently) is remarkable. For H_2O contents less than the 0.6% stored in muscovite, the rock would exist as a vapor-absent assemblage separated by a vertical phase boundary from the vapor-present assemblage.

The vapor-absent assemblage melts at a higher temperature than the vapor-present assemblage (compare Figures 3 and 2) as predicted from the synthetic system (Figure 1). For each pressure, for the anhydrous rock composition, there is a third solidus temperature in the region of 1125°C at 15 kbar, and 1210°C at 25 kbar [*Huang and Wyllie*, 1975]. At low pressures, where the vapor phase composition is almost pure H_2O, the vapor-present solidus curve and other phase boundaries are isothermal. At high pressures, where the vapor contains significant amounts of dissolved rock, they are not quite isothermal, as shown in Figure 5, and by *Stern and Wyllie* [this issue, Figures 2 and 3]. For discussion see *Robertson and Wyllie* [1971] and *Whitney* [1975].

The H_2O-saturation boundary separates phase fields with vapor from those without vapor. In the vapor-absent region, the upper stability limits for quartz, feldspars, jadeite and garnet decrease considerably with increasing H_2O content. The muscovite breakdown temperature increases with decreasing H_2O content, reaching the very low H_2O contents where muscovite granite melts in the absence of vapor. The crystallization of muscovite from melts containing little H_2O is consistent with phase relationships in synthetic systems (Figure 1; *Yoder and Kushiro* [1969]; *Modreski and Boettcher* [1972,

TABLE 4. Experimental Runs for Muscovite Granite (L26) With No Water Added

Run	Pressure, kbar	Temperature, °C	Duration, Hours or Months (m)	Estimated % Liquid	Results Phases Present
23	2	650	4 (m)	0	Qz, Ab, Or, Ms, (Si), (Co), Ga
19	2	675	4 (m)	0	Qz, Ab, Or, Ms, (Si), (Co), Ga
25	2	700	7 (m)	0	Qz, Ab, Or, (Ms), (Si), (Co), Ga
21	2	725	3.5 (m)	<1	Qz, Ab, Or, (Si), (Co), Ga, (L)
393	10	725	12	0	Qz, Ab, Or, Ms, Ga
369	10	750	24	<1	Qz, Ab, Or, Ms, Ga, (L)
233	10	775	24	<1	Qz, Ab, Or, Ms, (Co), Ga, (L)
232	10	800	24	2	Qz, Ab, Or, Co, Ga, L
344	10	1025	23	40	Qz, Fsp, (Ky), Co, L
345	10	1075	24	80	Qz, Co, L
259	10	1150	10	80	Qz, (Si), (Co), L
258	10	1200	10	98	(Qz), (Si), (Co), L
262	10	1250	2.5	99	(Qz), Si?, (Co), L
257	15	800	23	0	Qz, Ab, Or, Ms, Ga
236	15	825	23	1	Qz, Ab, Or, (Ms), (Co), Ga, (L)
230	15	875	25	3	Qz, Fsp, Co, Ga, L
241	15	1000	3	5	Qz, Fsp, Co, Ga, L
269	15	1000	43	8	Qz, Fsp, Co, L
266	15	1050	42	25	Qz, Fsp, (Ky), Co, L
265	15	1100	47	75	Qz, Ky?, Si?, (Co), L
263	15	1200	37	80	Qz, Si, L
296R	15	1315	5	...	...
	15	1200	5	99.5	Co?, L
247	15	1250	5	96	(Qz), (Si), Co, L
254R	15	1315	5	...	...
	15	1240	5	98	(Si), (Co), L
249	15	1300	5	99	(Co), L
252	25	850	20	0	Qz, Jd, Or, Ms, Ga
396	25	875	12	...	Qz, Jd, Or, Ms, Ga
253	25	900	22	1	Qz, Fsp, (Ky), Co, Ga, (L)
356	25	950	10	2	Qz, (Ab), Fsp, Ms, (Ky), (Si), Co, Ga, L
351	25	1000	8	2	Qz, Fsp, (Ky), Co, Ga, L
338	25	1100	8	25	Qz, Fsp, (Ky), Co, L
339	25	1150	9	35	Qz, Fsp, (Ky), Co, L
326	25	1200	6.5	70	Qz, Ky, Co, L
256	25	1300	4	90	Qz, Ky, Co, L
255	25	1350	4	99	(Qz), (Co), L
260	35	925	20	0	Ct, Jd, Or, Ms, (Co), (Ga)?, OrH?
261	35	975	20	0	Ct, Jd, Or, (Ky), Co, OrH?
267	35	1025	23	0	Ct, Jd, Or, (Ky), Co
346T	35	900	6	...	...
	35	1075	18	1	Ct, Jd, Or, (Ky), Co, (L)
347T	35	900	6	...	...
	35	1150	26	10	Ct, Jd, (Fsp), (Ky), Co, L
341	35	1200	8	70	Qz, (Fsp), (Ky), Co, L
340	35	1250	14	80	Qz, (Ky), Co, L
268	35	1350	8.5	95	Qz, Ky, Co, L
345	35	1400	2	90	Qz, Ky, Co, L
364	35	1450	1/2	90	Qz, Ky, Co, L

Abbreviations: see Figure 1 and Table 3.

1973]). At 15 kbar, the orthoclase-out boundary terminates at about 860°C, where two coexisting feldspars are replaced by a single feldspar. At 25 kbar, the critical temperature occurs just above the reaction of jadeite. With increasing temperature, the feldspathic components exist as orthoclase + jadeite, orthoclase + albite through a narrow temperature interval, followed in turn by a single alkali feldspar.

At 15 kbar, traces of kyanite and metastable corundum exist above the heavy line marking the quartz-out boundary. At 25 kbar, kyanite phase fields extend from the muscovite-out boundary to temperatures of 100°C or more above the quartz-out boundary. The temperature of the kyanite-out boundary decreases as H_2O content decreases from 55% to 30% H_2O, which probably reflects the preferential solubility of alkalies in the vapor, compared with alumina and silica. Because kyanite is present only in trace amount, it seems appropriate to consider the upper stability limit of quartz as the liquidus, for comparison with the phase relationships of biotite-granite. The solubility of H_2O in the granite liquid, estimated by the intersections of the H_2O-saturation boundaries with the quartz liquidus, is 23±3% at 15 kbar, and 29±2% at 25 kbar.

Reactions can be reversed in the presence of H_2O-undersaturated liquids at 15 kbar and above. The quartz-out boundary with 9.5% H_2O at 15 kbar was reversed as shown in runs 284, 288, 382, and 289R, in the presence of traces of metastable corundum. The albite-jadeite reaction with 3-4.6% H_2O at 15 kbar was reversed as shown in runs 319, 315, and 322T.

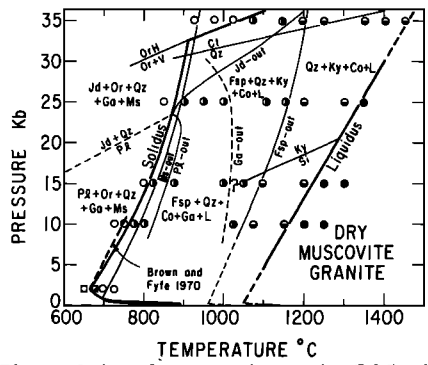

Fig. 3. Phase relations for muscovite granite (L26) with no water added, but 0.66% H_2O in the rock, stored in muscovite [*Huang and Wyllie,* 1973]. Experiments are listed in Table 4. The 2 kbar runs marked with square symbols were with excess H_2O. The dashed line is the solidus for a similar rock reported by *Brown and Fyfe* [1970]. Abbreviations: see Figure 1.

H_2O-Undersaturated Liquidus Surface

The liquidus surface corresponding to the quartz(coesite)-out phase boundary, neglecting the traces of kyanite, sillimanite, and corundum at higher temperatures, is given in Figure 6, with contours for constant H_2O contents. The limiting boundary for excess H_2O was taken from Figure 2, the contour for 0.6% H_2O was taken from Figure 3, and the dry liquidus boundary was estimated by taking the same slope as the 0.6% H_2O contour. The H_2O contours were passed through points from 15 kbar (squares) and 25 kbar (circles) taken directly from the quartz-out boundaries in Figures 4 and 5, respectively. The contours terminate on the excess-H_2O liquidus at crosses. The crosses were interpolated between the 15 kbar and 25 kbar solubilities determined at 15 kbar and 25 kbar, and calculated for lower pressures by *Huang* [1977], following the method of *Wasserburg* [1957] and using the data of *Burnham et al.* [1969] and *Burnham and Davis* [1971, 1974].

Muscovite coexists with quartz at or just below the liquidus with excess H_2O between about 5 kbar and 15 kbar, but with increasing pressure the quartz liquidus migrates to higher temperatures than the muscovite-out curve (Figure 2). Muscovite as a near-liquidus mineral does not extend across the H_2O-undersaturated liquidus surface, because of the divergence between the muscovite and quartz boundaries with decreasing H_2O content (Figures 4 and 5). At all pressures above 5 kbar, and probably at lower pressures where we have no results, kyanite, or sillimanite, or metastable corundum occurs on and above the H_2O-undersaturated quartz/coesite liquidus surface (Figures 2, 3, 4, and 5).

Microprobe Analyses of Phases at 15 kbar With 5% H_2O Added

Table 6 lists a series of runs conducted in gold capsules at 15 kbar specifically to prepare polished charges for electron microprobe determination of phase compositions for the 5% H_2O composition in Figure 4. The phases coexisting with glass are listed, according to the results given in Figure 4 and Table 5, and the average composition of glass determined from several analyses is given for each temperature.

The glasses analyzed were clear, free of minerals, and the consistency among analyses indicates that they were homogeneous. The glass compositions change fairly regularly with increasing temperature. The result at 800°C departs somewhat from the main trends, which are as follows. At 650°C and 700°C, SiO_2 is low, Al_2O_3 is high, and K_2O is high compared with the composition of the granite (Table 1). The glass compositions (anhydrous) are similar to that of syenite, which is consistent with the pressure effect on the composition of the eutectic in the residua system [*Huang and Wyllie,* 1975]. Between 700°C and 800°C, SiO_2 increases significantly towards granitic values, and Al_2O_3 drops markedly. Between 800°C and 900°C, the plagioclase dissolves, and Na_2O increases. If the difference between the total analyses and 100% is equated approximately to the H_2O content of the glass, and thus to that of the original H_2O-undersaturated liquid, the results indicate that dissolved H_2O changed from about 11–13% between 650°C and 800°C, with a decrease to about 7–8% associated with the increased melting where plagioclase and muscovite disappear between 800°C and 900°C. According to Figures 4 and 6, and 23% H_2O is required for saturation of the liquid at 15 kbar.

The average compositions of plagioclase crystals were determined at 650°C (6 analyses) and 700°C (10 analyses). The results in mole per cent anorthite were 5.9 at 650°C, and 5.1 at 700°C, essentially unchanged compared with the 5.1% in the original granite. The paragonite contents of muscovite from runs at 700°C and 750°C are, respectively, 5.9 and 3.7 mole per cent, compared with 6.7% in the muscovite of the original granite.

MUSCOVITE AND SILICATE-H_2O LIQUIDS

Phase relationships in the synthetic system K_2O-Al_2O_3-SiO_2-H_2O and the natural muscovite granite system illustrate the process of partial fusion of a rock containing a hydrous mineral but no free vapor, and outline the range of conditions under which muscovite will crystallize from H_2O-undersaturated silicate liquids. Figure 7 compares schematic phase relationships in T-X_{H_2O} diagrams at 2 kbar and 15 kbar for three different bulk compositions of increasing complexity: muscovite (invariant point Q_2 in Figure 1), muscovite + quartz (invariant point Q_1 in Figure 1) and muscovite granite (Figure 4). The amounts of H_2O stored in the crystalline assemblages are marked on the horizontal axes. For starting compositions with less H_2O than that required to constitute the maximum amount of muscovite, the vapor-absent assemblage includes muscovite and the products of the dehydration reaction.

At low pressures, muscovite dissociates at temperatures lower than the solidus, and melting begins for the anhydrous crystalline assemblage in the presence of H_2O vapor, with $P_{e_{H_2O}} = P_{total}$ (*Greenwood* [1961] for definition of $P_{e_{H_2O}}$). In Figures 7*a*, 7*b*, and 7*c* the point *a* gives the solubility of H_2O in the saturated liquid with composition of the mineral assemblage. The solidus reactions are univariant in Figures 7*a* and 7*b* (compare Figure 1), and melting is completed isothermally in the presence of vapor. For the muscovite granite in Figure 7*c*, vapor-present melting occurs through a temperature interval above the solidus. For mixtures with H_2O contents less than *a*, the assemblage passes through a vapor-absent region with $P_{e_{H_2O}} < P_{total}$. This region begins at the solidus for the univariant reactions, and at a temperature higher than the solidus for the more complex system (Figure 7*c*), the temperature interval increasing with H_2O content of the starting composition.

TABLE 5. Experimental Runs for Muscovite Granite (L26) at 15 kbar and 25 kbar With Water Contents Low Enough to Delineate the Vapor-Absent Regions

Run	Pressure, kbar	Temperature, °C	Wt. % H_2O	Duration, Hours	Results Phases Present
359	15	635	12	20	Qz, Ab, Ms, (Co), (Ga), L
357	15	660	9	22	Qz, Ab, Ms, L
353	15	660	12	23	Qz, Ms, L
374	15	700	1	23	Qz, Ab, Or, Ga, L
307	15	700	5	41	Qz, Ab, Ms, Ga, L
310	15	700	10	27	Qz, Ms, L
282	15	750	15	20	Qz, Ms, (Co), L
299	15	750	23	24	Qz, Ms, (Co), L
386	15	750	24	12	Qz, Ms, Co, L
301	15	750	25	22	Qz, (Ms), Co, L
293	15	775	15	22	Qz, Co, L
337	15	775	20	22	(Qz), Co, L
325	15	775	23	27	Ky, Co, L
303	15	795	5	20	Qz, Ab, Ms, Co, L
283	15	800	15	20	Qz, (Co), L
302	15	820	5	20	Qz, Ab, (Ms), Co, L
306	15	820	9	22	Qz, Co, L
292	15	825	15	23	Qz, Co, L
280	15	850	14	20	Co, L
388	15	850	3.2	18	Qz, Ab, Co, (Ga), L
390	15	875	2.7	10.5	Qz, Fsp, Co, Ga, L
382	15	875	5	10	Qz, Co, L
289R	15	940	9.5	9	...
	15	875	...	11	Qz, Co, L
288	15	900	9.5	11	Qz, Co, L
279	15	900	15	20	Co, L
284	15	925	9.5	9	(Si)?, Co, L
354	15	950	5	23	Qz, (Si)?, (Co), L
363	15	1000	5	5	Qz, Co, L
501	15	1125	1.6	23	Qz, Co, L
502	15	1175	1.6	23	Co, L
392T	25	595	5	5	...
	25	630	...	6	Qz, Jd, Ms
389T	25	595	10	5.5	...
	25	630	...	6	Qz, Jd, Ms
379T	25	595	10	5	...
	25	650	...	15	Qz, Jd, Ms, (L)
377	25	675	10	15	Qz, Jd, Ms, L
504	25	725	5	32	Qz, Jd, Ms, L
360	25	720	16	20	Qz, Jd, Ms, L
372	25	750	1.6	21	Qz, Jd, (Or), Ms, L
320T	25	595	3	6	...
	25	750	...	39	Qz, Jd, Ms, L
313T	25	595	10	11.5	...
	25	725	...	5	...
	25	750	...	21	Qz, Jd, Ms, L
318T	25	595	13	6	...
	25	750	...	18	Qz, Jd, Ms, L
397	25	770	20	13	Qz, (Ky), L
352	25	770	25	20	Qz, (Ms), Ky, L
362	25	775	15	11	Qz, Ms, L
316T	25	595	15	15	...
	25	800	...	25	Qz, Ky, L
503	25	820	5	24	Qz, Jd, Ms, L
391	25	825	0.5	10.5	Qz, Jd, Or, Ms, L
315	25	850	4.6	24	Qz, Jd, Ms, L
368	25	855	25	18	Ky, L
319	25	875	4.5	24	Qz, Ab, (Ms), Ky, L
298	25	875	20	18	Qz, Ky, L
295	25	875	25	15	Ky, L
322T	25	850	3	24	...
	25	885	...	24	Qz, Ab, (Ms), Ky, L
297	25	900	20	15	Ky, L
394	25	910	3.3	5.5	Qz, Fsp, Ky, L
291	25	925	20	15	Ky, L
309	25	925	25	16	Ky, L
378	25	950	5	19	Qz, Ms, L
375	25	950	7.3	18	Qz, Ky, L
311	25	950	25	15	(Ky), L
286	25	975	10	6	Qz, Ab, Ky, L
287	25	1025	9.5	6	Qz, Ky, L
371	25	1025	23	22	(Ky), L

TABLE 5. (continued)

Run	Pressure, kbar	Temperature, °C	Wt. % H_2O	Duration, Hours	Results Phases Present
294	25	1050	10	10	Ky, L
290	25	1075	10	6	Ky, L
398	25	1075	21.5	12	(Ky), L
365	25	1100	5	5	Qz, Ky, L
308	25	1125	10	0.5	Qz, (Ky), Co, L
312	25	1125	10	6	Ky, L
367	25	1225	10	10	Co?, L

Abbreviations: see Figure 1 and Table 3.

At the pressures corresponding to the invariant points in Figure 1, the temperature of a dehydration reaction reaches that of a solidus reaction. The shaded areas in Figure 7 show where at higher pressures the muscovite is stable at temperatures above the solidus. At 15 kbar, the vapor-absent melting reactions in Figures 7*d* and 7*e* are located at temperatures higher than the vapor-present reactions, following the univariant reactions in Figure 1. The same condition exists for the muscovite granite in Figure 7*f*, as determined in Figures 2, 3, and 4.

Each melting reaction in Figures 7*d* and 7*e* is univariant, but dissociation products of muscovite occur at temperatures above each reaction. The vapor-present solidus reactions produce liquid saturated with H_2O. For mixtures with more H_2O than that represented by points *a* muscovite melts completely at the solidus, but for mixtures with less H_2O muscovite persists with other minerals and H_2O-undersaturated liquid through an interval extending to the vapor-absent solidus temperature. The muscovite-out boundaries *ab* connect the two solidus reactions through the vapor-absent region, with $P_{e_{H_2O}} < P_{total}$. For the muscovite granite at 15 kbar (Figure 7*f*), the vapor-absent region is bounded below by a line diverging from the solidus with increasing H_2O content (as in Figure 7*c*), and by the muscovite-out curve rising through the vapor-absent region to the vapor-absent solidus reaction. Muscovite persists through a considerable temperature interval above the vapor-present solidus. The liquid produced by the melting of vapor-absent muscovite granite is H_2O-undersaturated, corresponding to the liquid associated with points *b* in Figures 7*d* and 7*e*.

It is not necessary for a silicate liquid to be sautrated with H_2O in order to precipitate muscovite, or any other hydrous mineral. The assemblage H_2O-undersaturated liquid + muscovite + other minerals exists in the shaded areas in Figure 7. Therefore, muscovite can be precipitated from an initial liquid with very low H_2O contents (compare biotite in *Stern and Wyllie* [this issue, Figure 6], after *Maaløe and Wyllie* [1975]).

The vapor-absent regions in synthetic and natural systems are illustrated in Figure 7. However, because $P_{e_{H_2O}}$ can vary from P_{total} to zero in these regions, it would be useful to map them in terms of $P_{e_{H_2O}}$. In natural systems, reactions may occur in the presence of multicomponent pore fluids, so that even in vapor-present systems, $P_{e_{H_2O}}$ may be much lower than P_{total}. Detailed theoretical treatments for dissociation reactions have been presented by *J. B. Thompson* [1955] and *Greenwood* [1961, 1967], but there is little information about melting reactions because of the paucity of thermodynamic data for liquids.

Dissociation and Melting of Muscovite With $P_{e_{H_2O}} < P_{total}$

Greenwood [1961] constructed a generalized three-dimensional P_{total}-$P_{e_{H_2O}}$-T model for the dissociation reactions of hydrous minerals. Figure 8 is a similar phase diagram constructed to illustrate the dissociation and melting reactions of muscovite around the invariant point Q_2 in Figure 1, with $P_{e_{H_2O}}$ as an additional independent variable. Figure 9 gives projections of the surfaces from within the model, contoured in terms of $P_{e_{H_2O}}$. *Greenwood*'s [1961] thermodynamic treat-

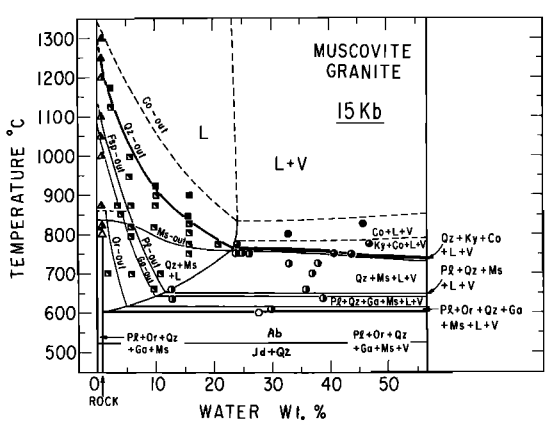

Fig. 4. Phase relations for muscovite granite (L26) with varying H_2O contents at 15 kbar (modified after *Huang and Wyllie* [1973]). Experiments are listed in Tables 3, 4, and 5. Abbreviations: see Figure 1. Circles—vapor present; squares and triangles—vapor absent; triangles—dry rock starting material.

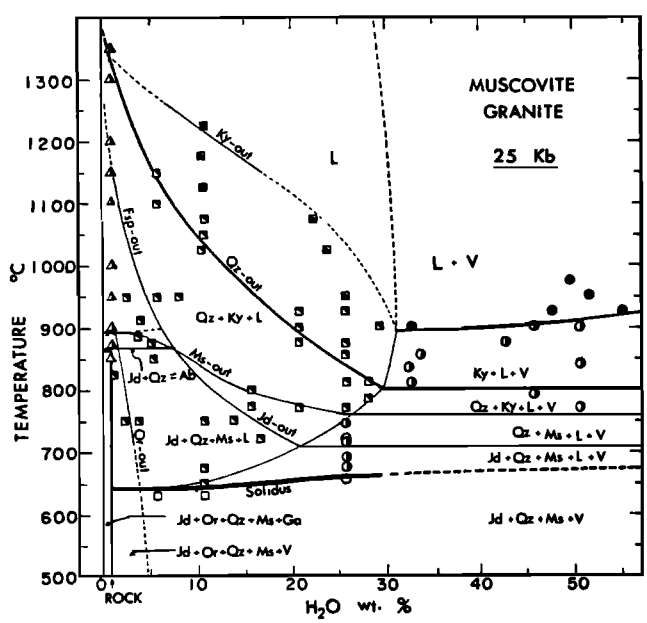

Fig. 5. Phase relations for muscovite granite (L26) with varying H_2O contents at 25 kbar [after *Huang*, 1977]. Experiments are listed in Tables 3, 4, and 5. Abbreviations: see Figure 1. Symbols: see Figure 4.

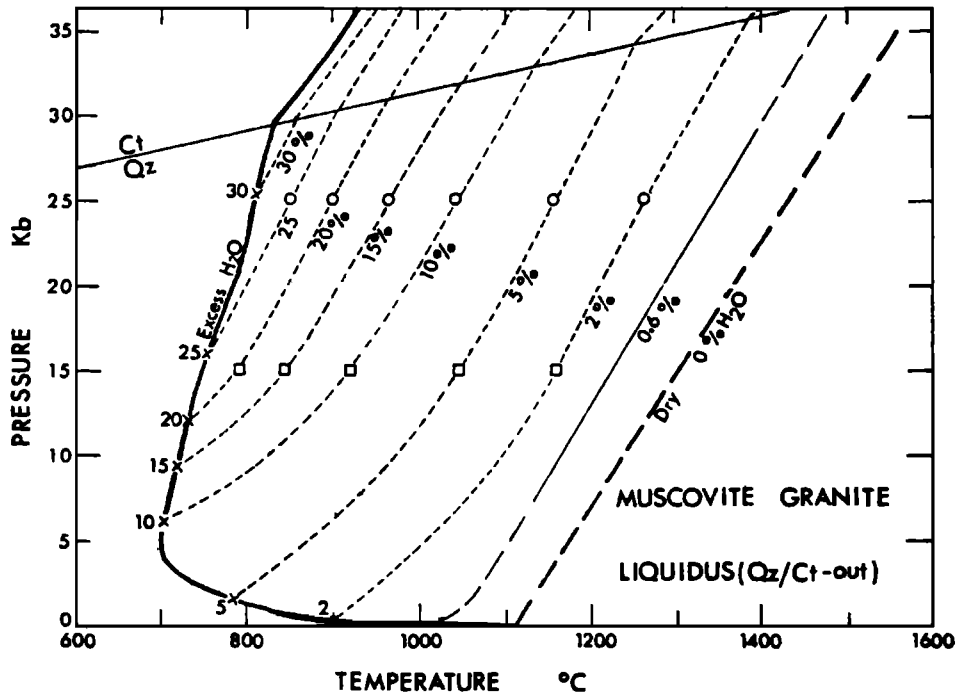

Fig. 6. The H_2O-undersaturated liquidus surface for muscovite granite (L26), neglecting the small amounts of aluminosilicate minerals existing at higher temperatures (Figures 2, 4, and 5). The surface connects the excess-H_2O quartz/coesite-out boundary (Figure 2) with the estimated position of the anhydrous liquidus. The surface is contoured by lines of constant H_2O content, and mapped with areas of primary crystallization of quartz and coesite. Muscovite is almost coincident with the excess-H_2O boundary between 5 kbar and 10 kbar (Figure 2). Abbreviations: see Figure 1.

ment of $P_{e_{H_2O}}$ involved an osmotic system. In the system K_2O-Al_2O_3-SiO_2-H_2O, $P_{e_{H_2O}}$ can be varied independently only if P_{vapor} can be reduced relative to P_{total}. This condition exists with vapor-absent H_2O-undersaturated liquid.

In Figure 8*c*, the univariant reactions around Q_2 are reproduced from Figure 1, together with the anhydrous fusion curve for Or + Co. The five phases Ms + Or + Co + L + V coexist at point Q_2. Each reaction curve involves four of these

TABLE 6. Electron Microprobe Analyses of Glass From Runs on Granite (L26) With 5 wt % Water Added at 15 kbar, Using Gold Capsules

Run	506	509	505	507	508	510
Temperature, °C	1000	950	900	800	700	650
Duration, hours	9	7	25	48	102	141
No. of analyses	4	5	6	7	5	4
Coexisting phases	Qz, Co	Qz, (Co)	Qz, Co	Ms, Pl, Qz, Co	Ms, Pl, Qz, Ga	Ms, Pl, Qz, Ga
SiO_2	71.8	70.9	69.5	70.8	54.0	56.9
TiO_2	...	...	...	...	...	0.06
Al_2O_3	12.9	13.0	14.3	11.7	23.5	19.3
Cr_2O_3	...	...	...	...	...	...
FeO	0.3	0.4	0.4	0.8	1.1	1.3
MnO	...	...	...	...	...	...
MgO	...	...	...	...	...	...
CaO	0.6	0.5	0.5	0.7	0.6	0.6
Na_2O	3.7	4.1	4.5	1.8	2.5	3.2
K_2O	3.1	3.1	3.5	3.10	6.3	5.5
Total	92.3	92.1	92.7	88.9	88.0	86.9
	Recalculated to 100% Total					
SiO_2	77.8	77.1	75.0	79.6	61.4	65.5
TiO_2	...	...	...	...	...	0.07
Al_2O_3	14.0	14.1	15.4	13.2	26.7	22.2
Cr_2O_3	...	...	...	...	...	...
FeO	0.3	0.5	0.4	0.9	1.3	1.5
MnO	...	...	...	...	...	...
MgO	...	...	...	...	...	...
CaO	0.6	0.6	0.6	0.8	0.7	0.7
Na_2O	4.0	4.5	4.9	2.0	2.8	3.7
K_2O	3.3	3.3	3.7	3.5	7.2	6.3

Abbreviations: see Figure 1 and Table 3.

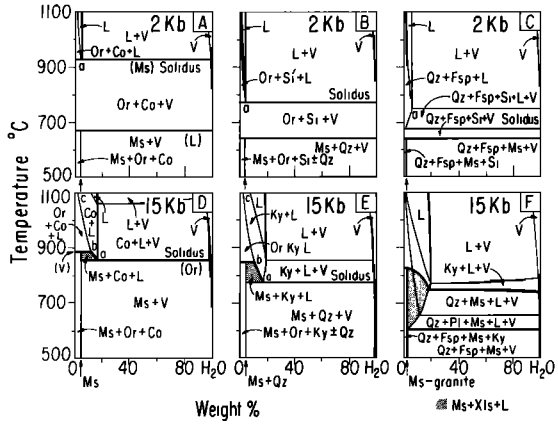

Fig. 7. Isobaric diagrams comparing the geometry of the melting relationships for muscovite-H_2O and muscovite+quartz-H_2O with that for muscovite-granite-H_2O at 2 kbar and 15 kbar (compare Figure 4). Abbreviations: see Figure 1.

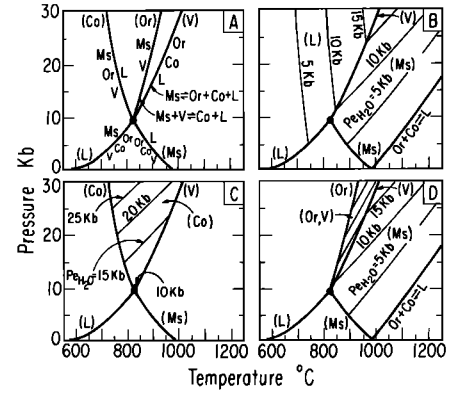

Fig. 9. P_{total}-T projections of the divariant surfaces from within the model of Figure 8*a*, illustrated by the contours for constant $P_{e_{H_2O}}$. The surface (Or, V) connects the reactions *a* and *b* in Figure 8*c*, and corresponds to the vapor-absent phase boundary *a-b* in Figure 7*a*. Abbreviations: see Figures 1 and 8.

phases, and it is identified by the fifth, missing phase, placed in parentheses. The reactions (Or) and (V) are the reactions identified by *a* and *b*, respectively, in Figure 7*d*. The five reactions around Q_2 are plotted in Figure 8*a* in a model with $P_{e_{H_2O}}$ as a third orthogonal axis, and with the diagonal plane representing the condition $P_{e_{H_2O}} = P_{total}$. The four reactions with excess vapor from Figure 8*c* are situated on this diagonal plane, as illustrated in the projection in Figure 8*b*. The vapor-absent melting curve for muscovite, (V), extends upwards from Q_2 into the region where $P_{e_{H_2O}} < P_{total}$, as shown clearly in projection in Figure 8*b*, and somewhat less clearly in Figure 8*a*.

The vapor-absent fusion curve for muscovite, (V), is connected to each of the other three univariant fusion curves by divariant surfaces within the model of Figure 8*a*. The divariant surface (L) extending from the subsolidus dehydration reaction also terminates along the line (V). These four

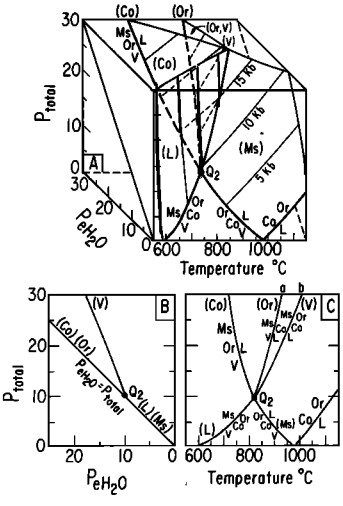

Fig. 8. Schematic diagram showing dehydration and melting reactions involving muscovite in the system K_2O-Al_2O_3-SiO_2-H_2O, including the conditions $P_{e_{H_2O}} < P_{total}$. Abbreviations: see Figure 1. Parentheses identify a phase assemblage in terms of the phase(s) absent from the invariant 5-phase assemblage at Q_2. Pressure axis is in kilobars. (*a*) P_{total}-$P_{e_{H_2O}}$-T diagram, showing the diagonal surface for $P_{e_{H_2O}} = P_{total}$. (*b*) Projection of univariant reactions, showing that reactions (Co), (Or), (Ms), and (L) coincide with projection of the $P_{e_{H_2O}} = P_{total}$ plane, whereas the vapor-absent reaction (V) is inclined to the plane. (*c*) Projection of univariant reactions onto the P_{total}-T face (compare Figure 1), together with the anhydrous melting curve.

surfaces are situated within the volume for $P_{e_{H_2O}} < P_{total}$ (Figures 8*a* and 8*b*), and their geometrical positions can be illustrated by contours for constant values of $P_{e_{H_2O}}$, as shown in Figure 8*a*. In Figure 9, the four divariant reaction surfaces are more clearly distinguished in projections; each univariant reaction is identified in Figure 9*a*, and each corresponding contoured surface from Figure 8*a* is projected onto the front P_{total}-T face of the model.

Figure 9*b* shows the projection of the two divariant surfaces (L) and (Ms) together with curve (V), along which they intersect. The slopes of $P_{e_{H_2O}}$ contours for (L) are assumed to be similar to those presented for the dissociation of muscovite + quartz by *Kerrick* [1972]. The intersections of these contours with the reaction curve (V) gives $P_{e_{H_2O}}$ values along (V). The $P_{e_{H_2O}}$ contours for the reaction (Ms) were drawn assuming the same slope as that for a syenite solidus surface [*Millhollen*, 1971] which is intermediate between results calculated for granite by *Kerrick* [1972] and for albite by *Burnham and Davis* [1974]. Contours on the surfaces (Co) and (Or, V) were drawn to connect values on the reaction curve (V) to the corresponding P_{total} pressures on the univariant curves (Co) and (Or), respectively (Figures 9*c* and 9*d*).

The divariant dehydration surface (L) in Figures 8*a* and 9*b* shows how reduction of $P_{e_{H_2O}}$ lowers the dissociation temperature at a given total pressure. The univariant reactions (Ms) and (Co) in Figure 8 show the beginning of melting in the system with excess H_2O, for the melting of assemblages Or + Co and Or + Ms. The divariant surfaces (Ms) in Figures 9*b* and 9*d*, and (Co) in Figure 9*c*, show how reduction of $P_{e_{H_2O}}$ increases the temperature of beginning of melting at a given total pressure. All H_2O is dissolved at these surfaces, giving H_2O-undersaturated liquids.

The vapor-absent divariant melting surface (Or, V) of Figures 8*a* and 9*d* is the liquidus for the assemblage Ms + Co. The line *ab* in Figure 7*d* corresponds to the 15 kbar section through this surface. At constant pressure, Figure 9*d* shows that $P_{e_{H_2O}}$ decreases, as the maximum temperature stability of Ms + Co + L increases from the H_2O-saturated melting of muscovite (Or) to its vapor-absent melting reaction (V). This is accompanied by a decrease in H_2O content of the liquid (Figure 7*d*).

The effect of decreasing $P_{e_{H_2O}}$ on muscovite stability therefore differs depending on the reaction. For subsolidus dehydration, (L), the temperature of muscovite reaction is lowered

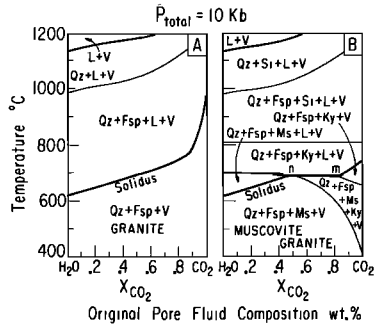

Fig. 10. The effect of H_2O-CO_2 mixtures on the melting relationships of granite at 10 kbar in a closed system, with initial subsolidus vapor phase compositions given by the horizontal axis, and initially 2% vapor present. Partly schematic: see text for method of construction. It is assumed that CO_2 solubility in granitic liquids is negligible [*Wyllie and Tuttle*, 1959; *Mysen et al.*, 1976]. Abbreviations: see Figure 1. (*a*) Simple granite without hydrous minerals. (*b*) Muscovite granite. The dissociation of muscovite enriches the vapor in H_2O, lowering the solidus towards the CO_2 side compared with the simple granite. Compare *Kerrick* [1972, Figure 5].

(Figure 9*b*); for vapor-absent melting, (Or, V), the temperature of muscovite stability is increased (Figure 9*d*).

The divariant reactions shown in Figures 8 and 9 are valid for the plotted values of $P_{e_{H_2O}}$, whatever the mechanism for producing these values. During metamorphism, the condition $P_{e_{H_2O}} < P_{total}$ is commonly achieved by the presence of a mixed pore fluid, such as H_2O-CO_2. Conditions on the dehydration surface, all three fusion surfaces, and the univariant reaction (V) can therefore be attained in the presence of vapor of appropriate compositions.

Buffering Effect of Muscovite on the Solidus of Granite-H_2O-CO_2

Figure 10 compares the phase relationships for granite and muscovite granite in closed systems at 10 kbar, with $P_{e_{H_2O}} < P_{total}$ achieved by diluting H_2O with CO_2. Each system has 2% pore fluid at low temperatures, with the original pore fluid composition given by the horizontal axis. With increasing temperature, melting or dissociation begins, and the vapor phase then changes in composition and amount and is no longer represented by the horizontal scale. The solidus and liquidus for pure H_2O are taken from Figures 2 and 6 (2% H_2O contour for H_2O-undersaturated liquidus surface).

The solidus in Figure 10*a* is based on calculation of $P_{e_{H_2O}}$ at the corresponding P_{total}, temperature, and mole fraction of H_2O in H_2O-CO_2 mixtures, from the thermodynamic properties of H_2O [*Burnham et al.*, 1969], following the method of *Millhollen* [1971]. The calculations assume ideal mixing of H_2O and CO_2, negligible solubility of CO_2 in the silicate melt, and no carbonate phases stable. The slope of the solidus curve is intermediate between that calculated for granite melting by *Kerrick* [1972] and for albite by *Burnham and Davis* [1971, 1974]. The solidus for granite-CO_2 is high, effectively the same as that for granite alone. Figure 10*a* shows that addition of very little H_2O to the pore fluid is sufficient to cause a large depression of the solidus temperature. In contrast, the addition of CO_2 to an aqueous pore fluid is much less effective in raising the solidus temperature.

The solidus for muscovite granite in Figure 10*b* with pore fluids from H_2O to *n* is effectively the same as that in Figure 10*a* [compare *Stern and Wyllie*, this issue; *Huang and Wyllie*, 1975]. For pore fluids richer in CO_2 than point *n*, however, muscovite begins to dissociate at temperatures below the solidus. Dehydration of muscovite in a close system changes the pore fluid compsoition towards H_2O. The muscovite dissociates through an isobaric divariant interval, beginning along the curve which intersects the solidus at point *n*. For a rock with original pore fluid composition between *n* and *m*, dissociation of muscovite drives the pore fluid composition to *n*, at which point melting begins. This is represented by the isothermal solidus line *n*-*m*. For original pore fluids with more CO_2 than point *m*, all muscovite is dissociated with pore fluid composition richer in CO_2 than point *n*, and the solidus temperature is therefore at some higher temperature than *n*, corresponding to a point on the solidus of Figure 10*a*. The solidus temperature never reaches the high values for granite-CO_2 shown in Figure 10*a*, because the dissociation of muscovite maintains a relatively high value of H_2O/CO_2 in the pore fluid.

For muscovite granite in the presence of pore fluids with a range of compositions (*n*-*m* in the specific example of Figure 10), the solidus temperature is buffered by the muscovite dehydration. The conditions for the beginning of melting are defined by the temperature and pore fluid composition at the intersection point, *n*. The locus of point *n* in *P*-*T*-*X* space is a univariant vapor-buffered curve on the solidus surface for muscovite-granite-H_2O-CO_2, representing the intersection of the divariant solidus surface for the rock with the divariant subsolidus dehydration surface for muscovite in this assemblage. The geometry and principles are the same as those described for solidus reactions buffered by amphibole, phlogopite, and dolomite in the system peridotite-H_2O-CO_2 [*Wyllie*, 1977*b*, 1978, 1979; *Eggler*, 1978].

The principle of the involvement of muscovite in granite melting is illustrated in terms of $P_{e_{H_2O}}$ (regardless of mechanism for reducing $P_{e_{H_2O}}$ relative to P_{total}) by the intersection of two divariant surfaces in Figure 8*a*. For the condition $P_{e_{H_2O}} < P_{total}$, the subsolidus dehydration of muscovite is represented by the surface (L). This surface meets the muscovite-bearing solidus surface (Co) along the univariant vapor-absent reaction (V). In Figure 10*b*, the corresponding isobaric curves for the solidus and muscovite dehydration (with $P_{e_{H_2O}} < P_{total}$ achieved by diluting H_2O with CO_2) meet at the isobaric invariant point *n*. The muscovite-absent solidus curve rising from *m* in Figure 10*b* corresponds to a portion of the solidus surface (Ms) extending from (V) in Figure 8*a*. Values of $P_{e_{H_2O}}$ on curve (V) in Figure 8 define the values in the H_2O-CO_2 fluids on the corresponding vapor-present buffered solidus curve. At higher temperatures, because of the artificial conditions set up for Figure 10, further analogy with Figure 8 becomes complicated.

The variations in X_{H_2O} and $P_{e_{H_2O}}$ illustrated in Figures 7, 8, 9, and 10 can also be expressed in terms of activity of H_2O (a_{H_2O}). *A. B. Thompson and Algor* [1977] have calculated *P*-*T*-a_{H_2O} paths for melting and crystallization in systems modelling muscovite granite and pelitic rocks, with particular reference to the effect of excess Al_2O_3 relative to the residua system, Ab-Or-Qz-H_2O.

Discussion

Much of the discussion of *Stern and Wyllie* [this issue] for the biotite granite is directly applicable to this muscovite granite, because the phase relationships are basically similar. The main difference is associated with the 4.8% normative co-

rundum in this rock, compared with none in the biotite granite, and with the differing reactions of 13.8% muscovite compared with only 4.7% biotite.

With excess H_2O, the solidus and the interval to the quartz/coesite-out boundary are almost the same in both rocks. The biotite survives through only a short temperature above the solidus and only at pressures below 10 kbar. The muscovite is a near-liquidus mineral between about 5 kbar and 10 kbar, and persists to at least 35 kbar, the highest pressure of experiments.

The H_2O-undersaturated liquidus surface for the biotite granite, dominated by quartz/coesite with plagioclase present only at low pressures and high temperatures, is similar in position and shape to the quartz/coesite surface in the muscovite granite. In the latter rock, kyanite or sillimanite and metastable corundum are produced in addition to quartz/coesite surface.

Stern and Wyllie [this issue] reviewed the eutectic-like character of biotite granite with excess H_2O up to about 5 kbar, and the loss of this character at higher pressures. Figure 2 illustrates the same characteristics for the muscovite granite. Note, however, that the melting interval at low pressures is about 100°C, which is not strictly 'eutectic' behavior. The determination that liquids at 650°C and 700°C at 15 kbar are syenitic (Table 6) confirms the explanation of this change in terms of migration of the eutectic composition in the feldspar-quartz Residua System away from SiO_2 with increasing pressure [*Huang and Wyllie,* 1975].

Stern and Wyllie [this issue] also emphasized that the eutectic-like condition exists only with excess H_2O. With less H_2O present than that required to saturate the liquid, there is a wide temperature interval between solidus and liquidus, as illustrated for the muscovite granite in Figures 3, 4, and 5.

Experimental results for both granites confirm that biotite and muscovite can be precipitated from H_2O-undersaturated liquids in magmas (liquid + crystals) with very low H_2O contents, at pressures ranging from low values where the hydrous mineral stability curve crosses the excess-H_2O solidus, to the highest pressures where the hydrous mineral is stable above the solidus. A significant H_2O limit is given by the geometrical boundary for the subsolidus tie-figure including the hydrous mineral without vapor. This amount of H_2O is marked in Figures 4, 5, and 7 by the vertical lines separating vapor-absent from vapor-present subsolidus assemblages. For magmas with H_2O contents less than this limit, a trace of hydrous mineral is produced as the vapor-absent liquid solidifies. The details depend on whether the hydrous mineral melts congruently or incongruently in the mineral assemblage [*Robertson and Wyllie,* 1971]. For magmas with H_2O contents greater than this limit, precipitation of the hydrous mineral is followed through a temperature interval by the coprecipitation of other minerals from the vapor-absent assemblage until vapor exsolution occurs, followed by crystallization of the H_2O-saturated liquid at the vapor-present solidus.

There is a misconception prevalent in the literature that hydrous minerals can be precipitated only from magmas with several per cent of H_2O. In his discussion of the crystallization of hydrous minerals from silicate melts, *Burnham* [1979, pp. 90–91] wrote: 'Therefore, the minimum value of X_m^w at which hornblende can exist stably with melt in this system is approximately 0.3 which is roughly equivalent to 3.0 wt. % H_2O. This minimum H_2O content is almost independent of magma composition, and, from the work of *Yoder and Kushiro* [1969], also appears to hold for biotite.' This does not mean that an original liquid must contain at least 3% H_2O in order to precipitate hydrous minerals within the crystallization interval, a view maintained by some petrologists. Using Figure 7*e* as an example, it means that the H_2O content of the H_2O-undersaturated liquid associated with the assemblage Ms + Or + Ky + L at temperature *b* is at least 3% (compare the corresponding reaction for muscovite granite in Figure 7*f*). Consider the phase assemblage at a temperature just above *b*. Because the assemblage Or + Ky + L contains H_2O content given by point *b*, the vapor-undersaturated liquid contains somewhat more H_2O than *b*, the precise amount depending on the proportion of liquid to crystals. It is this liquid which then precipitates muscovite. This is the liquid discussed by *Burnham* [1979], with the limit of at least 3% H_2O. This is a liquid within a magma composed to liquid + crystals, but note from Figure 7*e* that this assemblage can be derived from original high-temperature liquids with H_2O contents ranging from *b* to almost 0%. What varies with original H_2O content is the percentage of H_2O-undersaturated liquid of defined composition at the temperature *b*.

Whether the activity of H_2O is reduced to low levels by small amounts of H_2O in a vapor-absent system, or by high CO_2/H_2O in a vapor-present system, the preceding discussion demonstrates how muscovite, biotite, or amphibole can be precipitated from normal silicate magmas with H_2O contents certainly as low as 0.5% (corresponding to the subsolidus boundary for maximum hydration). At the stage of initial precipitation, *Burnham's* [1979] work indicates that the H_2O content of the H_2O-undersaturated liquid in the magma exceeds 3%. This limit must vary as a function of pressure and bulk composition (and hence mineralogy).

Figures 7, 8, 9, and 10 permit some generalizations about the melting and stability of hydrous minerals such as muscovite, biotite, and amphibole if a_{H_2O} or $P_{e_{H_2O}}$ is decreased by increasing the ratio of CO_2/H_2O in the vapor phase: (1) the temperature of beginning of melting of mineral assemblages is increased, (2) the temperature of subsolidus dehydration of hydrous minerals is decreased, (3) the stability temperature of hydrous minerals coexisting with liquid is increased (to the maximum value where CO_2/H_2O gives a_{H_2O} corresponding to the vapor-absent melting reaction). For further examples, see *Eggler* [1972], *Holloway* [1973], *Eggler and Burnham* [1973], *Allen and Boettcher* [1978], and *Allen et al.* [1975].

The phase relationships can be used to test for conditions under which the muscovite granite could be a primary magma from various source rocks. The near-liquidus minerals for a primary magma must correspond to the major minerals in the source rock at the depth and temperature of origin. The liquidus minerals are sillimanite or kyanite, but there is a well-defined sub-liquidus surface for the coexistence of these minerals with quartz or coesite (Figures 2 to 6). Quartz or coesite crystallizes without feldspar through a considerable interval below the liquidus. The candidates for source rocks are mantle peridotite, subducted oceanic crust, and continental crust. Neither of the first two sources could yield granitic liquid with prominent, residual quartz/coesite. *Huang and Wyllie* [1973] used results for the muscovite granite to model the partial melting of marine sediments during subduction, and concluded that the products would not be primary granites or rhyolites. This conclusion is now confirmed by the analyses of glass from the partly melted rock at mantle pressures (Table 6).

It is well-established that H_2O-undersaturated granite liquid is a normal product of regional metamorphism of varied crustal rocks [e.g., *Wyllie, 1977a*]. For this muscovite granite to be a primary melt from the crust, it would have to be derived from a source rock leaving residual sillimanite. It could possibly represent a primary melt leaving residual muscovite and quartz under specific conditions (Figure 2): at depth corresponding to pressures between 5 kbar and 10 kbar, temperature of 700°C to 725°C, with sufficient H_2O to saturate the liquid with 9–16 wt. % H_2O (depending on the pressure, Figure 6). In fact, the high muscovite content (reflected in the high normative corundum) is sufficient to disqualify this bulk composition as a candidate for a primary melt from the crust. The available evidence suggests that only a few percent of muscovite is soluble in granite liquids at crustal pressures [*Lambert et al.*, 1969, Figure 5; *Wyllie, 1977a*, Figure 2]. Therefore, the mineralogy of this particular granite indicates either that it represents a granite melt with additional muscovite (possibly derived from restite material), or that it represents a melt from which a vapor phase has leached alkalies [e.g., *Tuttle and Bowen*, 1958, pp. 89–91; *Norton*, 1970].

The phase relationships for granitic and related rocks are consistent with the ideas of I-type and S-type granites [*Chappell and White*, 1974; *White and Chappell*, 1977], but the major-element relationships are not adequate to exclude alternative processes. Additional experiments related to the origin of S-type granites include those with pelitic sediments by Winkler and associates (see *Winkler* [1976] for a review), *Wyllie and Tuttle* [1961], *Kilinc* [1972], and *Green* [1976]. *Wyllie and Tuttle* [1961] melted five standard shales from Pennsylvania, varying widely in chemical composition, in the presence of excess H_2O at pressures up to 3 kbar. The solidus curves were 20°C to 40°C higher than the corresponding curve for granites. About 150°C above the solidus curves the shales were about 50% melted, and the refractive indices of the quenched glasses indicated that the liquid compositions were in the range granite-granodiorite. The melts were accompanied by residual refractory minerals including quartz, cordierite, hypersthene, muscovite, mullite, and calcic plagioclase.

Green [1976] tested the proposal that specific S-type granites were derived by partial melting of pelitic rocks. He confirmed that the fusion of pelitic rocks with 2% and 5% H_2O pressures of 4 kbar, 7 kbar, and 10 kbar produces granitic liquids. He compared Fe/Mg ratios in the liquids and residual cordierite and garnet with partition relationships in natural S-type granites, and concluded that the results were consistent with magma generation from the pelitic rocks at 800 ± 20°C (below the maximum stability of biotite), at depths greater than 25 km for garnet-bearing granites, and less than 25 km for cordierite-bearing granites (compare Figures 2 and 6 at 800°C and 7 kbar = 25 km).

The phase relationships for a single rock summarized in this paper provide constraints about its origin, but they do not provide an adequate basis for the petrogenesis of S-type granitoids. It is necessary to consider in addition the phase relationships of other rocks constituting a batholithic series, as well as the field relationships and the geochemistry of trace elements and isotopes. There is growing evidence from geochemistry and geophysics that few granites have a simple origin [e.g., *Atherton and Tarney*, 1979], and many batholiths contain evidence for the involvement of material from subducted oceanic crust, mantle, and continental crust [e.g., *Hamilton and Myers*, 1967; *Wyllie, 1977c*; *Burnham*, 1979].

Johannes [1980] concluded that most experimental results on granitic rocks at crustal pressures were metastable, and he raised an important question: To what extent is it valid to apply metastable experimental results on granitic rocks to natural processes? *Stern and Wyllie* [this issue] reviewed this topic, and agreed that the attainment and demonstration of reversible equilibrium is impossible in many parts of the multi-mineral granite systems. The failure to reach equilibrium with muscovite granite at 2 kbar in runs of 4 and 7 months duration is confirmed in Figures 2 and 3 (Tables 3 and 4). Some phase boundaries were reversed within 25°C at 15 kbar and 25 kbar, but metastable corundum was widely distributed. We endorse *Johannes'* [1980] conclusion, but we feel satisfied that the patterns of phase relationships that have emerged from many experimental studies on many compositions are applicable to petrological processes. They help to distinguish between possible and impossible processes. When it comes to tracing the specific compositions of feldspars and liquids in the low-pressure H_2O-undersaturated regions most directly applicable to the emplacement and crystallization of batholiths, however, experiments have not yet provided definitive information.

Another aspect of the equilibrium question, and the applicability of experimental data to real magmas, is provided by the crystal growth experiments of *Naney and Swanson* [1980] using model granitic compositions with added Fe-Mg components. They found that the mafic minerals (orthopyroxene, clinopyroxene, biotite, hornblende, epidote, and magnetite) nucleated and grew outside of their thermal stability fields as defined by equilibrium phase diagrams. In the undercooling crystal growth experiments, the nucleation of feldspars and quartz was greatly inhibited by the presence of Fe and Mg in the systems. They suggested that the border zones of granitic plutons may become enriched in mafic minerals by their more rapid nucleation and early crystallization rather than other processes of differentiation commonly proposed. *Johannes* [1980] suggested from his results with the felsic components that reaction rates are so slow that we should expect non-equilibrium processes to occur in the generation of granites as well as during their crystallization.

Acknowledgments. This research was supported by the Earth Sciences Section of the National Science Foundation, NSF grant EAR 76-20413. For review of earlier versions of parts of the manuscript we thank V. C. Juan, D. M. Kerrick, R. C. Newton, and Y. Wang.

REFERENCES

Allen, J. C., and A. L. Boettcher, Amphiboles in andesite and basalt, II, Stability as a function of P–T–f_{H_2O}–f_{O_2}, *Am. Mineral., 63*, 1074–1087, 1978.

Allen, J. C., A. L. Boettcher, and G. Marland, Amphiboles in andesite and basalt, I, Stability as a function of P–T–f_{O_2}, *Am. Mineral., 60*, 1069–1085, 1975.

Atherton, M. P., and J. Tarney (Eds.), *Origin of Granite Batholiths, Geochemical Evidence*, 148 pp., Shiva Publishing, Orpington, 1979.

Boettcher, A. L., and D. M. Kerrick, Temperature calibration in cold-seal vessels, in *Experimental Techniques in Non-Condensed Systems*, edited by G. C. Ulmer, pp. 178–193, Springer-Verlag, New York, 1971.

Brown, G. C., and W. S. Fyfe, The production of granite melts during ultrametamorphism, *Contrib. Mineral. Petrol., 28*, 235–244, 1970.

Burnham, C. W., Magmas and hydrothermal fluids, in *Geochemistry of Hydrothermal Ore Deposits*, 2nd ed., edited by H. L. Barnes, pp. 71–136, John Wiley, New York, 1979.

Burnham, C. W., and N. F. Davis, The role of H_2O in silicate melts, I,

P–V–T relations in the system $NaAlSi_3O_8$–H_2O to 10 kilobars and 1000°C, *Am. J. Sci., 270,* 54–79, 1971.

Burnham, C. W., and N. F. Davis, The role of H_2O in silicate melts, II, Thermodynamics and phase relations in the system $NaAlSi_3O_8$-H_2O to 10 kilobars, 700° to 1100°C, *Am. J. Sci., 274,* 902–940, 1974.

Burnham, C. W., J. R. Holloway, and N. F. Davis, The specific volume of water in the range of 1000 to 8900 bars, 20° to 900°C, *Am. J. Sci., 267-A,* 70–95, 1969.

Chappell, B. W., and A. J. R. White, Two contrasting granite types, *Pac. Geol., 8,* 173–174, 1974.

Eggler, D. H., Water-saturated and undersaturated melting relations in a Paricutin andesite and an estimate of water content in the natural magma, *Contrib. Mineral. Petrol., 34,* 261–271, 1972.

Eggler, D. H., The effect of CO_2 upon partial melting of peridotite in the system Na_2O-CaO-Al_2O_3-MgO-SiO_2-CO_2 to 35 kb, with an analysis of melting in a peridotite-H_2O-CO_2 system, *Am. J. Sci., 278,* 305–343, 1978.

Eggler, D. H., and W. C. Burnham, Crystallization and fractionation trends in the system andesite-H_2O-CO_2-O_2 at pressures to 10 kb, *Geol. Soc. Am. Bull., 84,* 2517–2532, 1973.

Green, T. H., Experimental generation of cordierite- or garnet-bearing granitic liquids from a pelitic composition, *Geology, 4,* 85–88, 1976.

Greenwood, H. J., The system of $NaAlSi_2O_6$-H_2O-argon: Total pressure and water pressure in metamorphism, *J. Geophys. Res., 66,* 3923–3946, 1961.

Greenwood, H. J., Mineral equilibria in the system MgO-SiO_2-H_2O-CO_2, in *Researches in Geochemistry,* vol. 2, edited by P. H. Abelson, pp. 542–567, John Wiley, New York, 1967.

Hamilton, W., and W. B., Myers, The nature of batholiths, *U.S. Geol. Surv. Prof. Pap., 554-C,* 30 pp., 1967.

Holloway, J. R., The system pargasite-H_2O-CO_2: A model for melting of a hydrous mineral with a mixed-volatile fluid, I, Experimental results to 8 kilobars, *Geochim. Cosmochim Acta, 37,* 651–666, 1973.

Huang, W. L., Melting and crystallization of hydrous granite at crust and mantle pressures, *Acta Geol. Taiwan., 19,* 13–28, 1977.

Huang, W. L., and P. J. Wyllie, Melting relations of muscovite-granite to 35 kbar as a model for fusion of metamorphosed subducted oceanic sediments, *Contrib. Mineral. Petrol., 42,* 1–14, 1973.

Huang, W. L., and P. J. Wyllie, Melting relations of muscovite with quartz and sanidine in the system K_2O-Al_2O_3-SiO_2-H_2O to 30 kilobars and an outline of paragonite melting relations, *Am. J. Sci., 274,* 378–395, 1974.

Huang, W. L., and P. J. Wyllie, Melting reactions in the system $NaAlSiO_3O_8$-$KAlSi_3O_8$-SiO_2 to 35 kilobars, dry and with excess water, *J. Geol., 83,* 737–748, 1975.

Huang, W. L., J. K. Robertson, and P. J. Wyllie, Melting relations of muscovite to 30 kbars in the system $KAlSi_3O_8$-Al_2O_3-H_2O, *Am. J. Sci., 273,* 415–427, 1973.

Johannes, W., Metastable melting in the granite system Qz-Or-Ab-An-H_2O, *Contrib. Mineral. Petrol., 72,* 73–80, 1980.

Kerrick, D. M., Experimental determination of muscovite + quartz stability with $P_{H_2O} < P_{total}$, *Am. J. Sci., 272,* 946–958, 1972.

Kilinc, I. A., Experimental study of partial melting of crustal rocks and formation of migmatites, *Proc. Int. Geol. Congr. 24th, Sect. 2,* 109–113, 1972.

Lambert, I. B., J. K. Robertson, and P. J. Wyllie, Melting reactions in the system $KAlSi_3O_8$-SiO_2-H_2O to 18.5 kilobars, *Am. J Sci., 267,* 609–626, 1969.

Maaløe, S., and P. J. Wyllie, Water content of granite magma deduced from the sequence of crystallization determined experimentally with water undersaturated conditions, *Contrib. Mineral. Petrol., 52,* 175–191, 1975.

Millhollen, G. L., Melting to nepheline syenite with H_2O and H_2O + CO_2, and the effect of dilution of the aqueous phase on the beginning of melting, *Am. J. Sci., 270,* 244–254, 1971.

Modreski, P. J., and A. L. Boettcher, The stability of phlogopite and enstatite at high pressures: A model for mica in the interior of the earth, *Am. J. Sci., 272,* 852–869, 1972.

Modreski, P. J., and A. L. Boettcher, Phase relationships of phlogopite in the system K_2O-MgO-CaO-Al_2O_3-SiO_2-H_2O to 35 kilobars: A better model for micas in the interior of the earth, *Am. J. Sci., 273,* 385–414, 1973.

Mysen, B. O., D. H. Eggler, M. G. Seitz, and J. R. Holloway, Carbon dioxide in silicate melts and crystals, I, Solubility measurements, *Am. J. Sci., 276,* 455–479, 1976.

Naney, M. T., and S. E. Swanson, The effect of Fe and Mg on crystallization in granitic systems, *Am. Mineral., 65,* 639–653, 1980.

Norton, J. J., Composition of a pegmatite, Keystone, South Dakota, *Am. Mineral., 55,* 981–1002, 1970.

Piwinskii, A. J., and P. J. Wyllie, Experimental studies of igneous rock series: A zones pluton in the Wallowa Batholith, Oregon, *J. Geol., 76,* 205–234, 1968.

Robertson, J. K., and P. J. Wyllie, Experimental studies on rocks from the Deboullie Stock, northern Maine, including melting relations in the water-deficient environment, *J. Geol., 79,* 549–571, 1971.

Seki, Y., and G. C. Kennedy, The breakdown of potassium feldspar, $KAlSi_3O_8$, at high temperatures and pressures, *Am. Mineral., 49,* 1688–1706, 1964.

Smith, J. V., X-ray-emission microanalysis of rock-forming minerals, I, Experimental techniques, *J. Geol., 73,* 830–864, 1965.

Stern, C. R., and P. J. Wyllie, Effect of iron absorption by noble-metal capsules on phase boundaries in rock-melting experiments at 30 kilobars, *Am. Mineral., 42,* 681–689, 1975.

Stern, C. R., and P. J. Wyllie, Phase relationships of I-type granite with H_2O to 35 kbar: The Dinkey Lakes biotite-granite from the Sierra Nevada Batholith, *J. Geophys. Res.,* this issue.

Thompson, A. B., Calculation of muscovite-paragonite-alkali feldspar phase relations, *Contrib. Mineral. Petrol., 44,* 173–194, 1974.

Thompson, A. B., and J. R. Algor, Model systems for anatexis of pelitic rocks, I, Theory of melting reactions in the system $KAlO_2$-$NaAlO_2$-Al_2O_3-SiO_2-H_2O, *Contrib. Mineral. Petrol., 63,* 247–269, 1977.

Thompson, J. B., Jr., The thermodynamic basis for the mineral facies concept, *Am. J. Sci., 253,* 65–103, 1955.

Tuttle, O. F., and N. L. Bowen, Origin of granite in the light of experimental studies in the system $NaAlSi_3O_8$-$KAlSi_3O_8$-SiO_2-H_2O, *Geol. Soc. Am. Mem., 74,* 153 pp., 1958.

Wasserburg, G. J., The effect of H_2O in silicate systems, *J. Geol., 65,* 15–23, 1957.

White, A. J. R., and B. W. Chappell, Ultrametamorphism and granitoid genesis, *Tectonophysics, 43,* 7–22, 1977.

Whitney, J. A., The effects of pressure temperature and X_{H_2O} on phase assemblages in four synthetic rock compositions, *J. Geol., 83,* 1–31, 1975.

Winkler, H. G. F., *Petrogenesis of Metamorphic Rocks,* 4th ed., Springer-Verlag, New York, 1976.

Wyllie, P. J., Crustal anatexis: An experimental review, *Tectonophysics, 43,* 41–71, 1977*a*.

Wyllie, P. J., Mantle fluid compositions buffered by carbonates in peridotite-CO_2-H_2O, *J. Geol., 85,* 187–207, 1977*b*.

Wyllie, P. J., From crucible through subduction to batholiths, in *Energetics of Geological Processes,* edited by S. K. Saxena and S. Battacharji, pp., 389–433, Springer-Verlag, New York, 1977*c*.

Wyllie, P. J., Mantle fluid compositions buffered in perioditite-CO_2-H_2O by carbonates, amphibole, and phlogopite, *J. Geol., 86,* 687–713, 1978.

Wyllie, P. J., Magmas and volatile components, *Am. Mineral., 64,* 469–500, 1979.

Wyllie, P. J., and O. F. Tuttle, Effect of carbon dioxide on the melting of granite and feldspar, *Am. J. Sci., 257,* 648–655, 1959.

Wyllie, P. J., and O. F. Tuttle, Hydrothermal melting of shales, *Geol. Mag., 98,* 56–66, 1961.

Yoder, H. S., and I. Kushiro, Melting of a hydrous phase: Phlogopite, *Am. J. Sci., 267-A,* 558–582, 1969.

(Received October 8, 1980;
revised March 19, 1981;
accepted March 20, 1981.)